

Sparsity-Aware Optimization of In-Memory Bayesian Binary Neural Network Accelerators

Prabodh Katti, Bashir M. Al-Hashimi, Bipin Rajendran
 Department of Engineering, King’s College London, London, UK
 Email: bipin.rajendran@kcl.ac.uk

Abstract—Bayesian Neural Networks (BNNs) provide principled estimates of model and data uncertainty by encoding parameters as distributions. This makes them key enablers for reliable AI that can be deployed on safety critical edge systems. These systems can be made resource efficient by restricting synapses to two synaptic states $\{-1, +1\}$ and using a memristive in-memory computing (IMC) paradigm. However, BNNs pose an additional challenge – they require multiple instantiations for ensembling, consuming extra resources in terms of energy and area. In this work, we propose a novel sparsity-aware optimization for Bayesian Binary Neural Network (BBNN) accelerators that exploits the inherent BBNN sampling sparsity – most of the network is made up of synapses that have a high probability of being fixed at ± 1 and require no sampling. The optimization scheme proposed here exploits the sampling sparsity that exists both among layers, i.e only a few layers of the network contain a majority of the probabilistic synapses, as well as the parameters i.e., a tiny fraction of parameters in these layers require sampling, reducing total sampled parameter count further by up to 86%. We demonstrate no loss in accuracy or uncertainty quantification performance for a VGGBinaryConnect network on CIFAR-100 dataset mapped on a custom sparsity-aware phase change memory (PCM) based IMC simulator. We also develop a simple drift compensation technique to demonstrate robustness to drift-induced degradation. Finally, we project latency, energy, and area for sparsity-aware BNN implementation in both pipelined and non-pipelined modes. With sparsity-aware implementation, we estimate upto $5.3\times$ reduction in area and $8.8\times$ reduction in energy compared to a non-sparsity-aware implementation. Our approach also results in $2.9\times$ more power efficiency compared to the state-of-the-art BNN accelerator.

Index Terms—Bayesian Neural Networks, Sparsity, In-Memory Computing, Phase Change Memory.

I. INTRODUCTION

Bayesian neural networks (BNNs) offer a key advantage by quantifying uncertainty in their predictions, which makes them more reliable, especially for risk-sensitive applications like diagnostics, surveillance, and autonomous vehicles [1], [2]. This prevents overconfident decisions, which is crucial in high-risk environments [3]. BNNs encode epistemic uncertainty by treating each parameter as a probability distribution, requiring ensemble predictors [4], [5]. However, this inference process is hardware-intensive as multiple instantiations are required for sampling [6], [7]. This paper explores efficiency gains by leveraging the inherent sparsity in Bayesian Binary Neural Networks, reducing the resource demands of ensembling.

Related Work: BNN accelerators on CMOS and FPGA have been explored [8], [9], but they face the ‘von Neumann bottleneck’, leading to high energy, area consumption, and latency

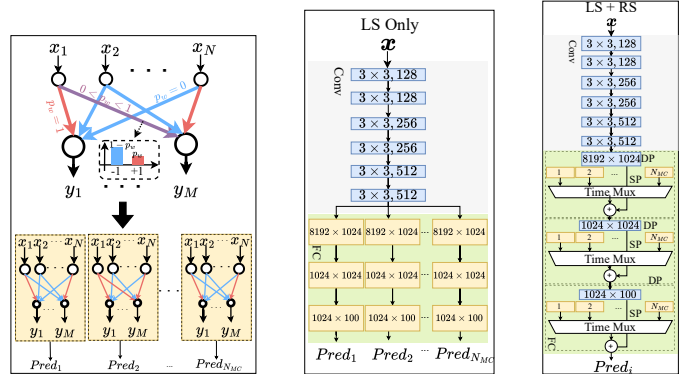


Fig. 1: **Left:** Illustration of BBNN inference, where only a small fraction of synapses are probabilistic and thus participate in sampling. **Center:** Sparsity-aware optimization to exploit the layer sparsity of VGGBinaryConnect (only synaptic layers shown here). Only layers with a significant concentration of probabilistic synapses are utilized to create an ensemble of predictions, all available simultaneously. **Right:** Utilizing parameter sampling sparsity within these layers by separating rows with probabilistic synapses into ‘Stochastic Plane (SP)’, and the rest into ‘Deterministic Plane (DP)’. The DP and one of the SP ensembles provide one set of predictions. Thus, predictions are available one by one.

due to excessive data movement [10]. In-memory computing addresses this by co-locating memory and processing, using crossbars of non-volatile devices like PCM, RRAM, STT-RAM, and SOT-MRAM [7], [11], enabling efficient matrix-vector multiplication through Ohm’s and Kirchhoff’s laws.

RRAM, PCM, STT-RAM, and SOT-MRAM have been used to implement Bayesian accelerators with Gaussian parameters [7], [11]–[13]. Nanoscale device stochasticity has also been considered as a resource to generate noise for sampling using the central limit theorem, though requiring additional hardware [7], [11]. In addition, these methods require Gaussian mean and standard deviation values to be stored per parameter. Architecture combining two devices to generate a Gaussian weight, co-locating entropy source and parameter storage was proposed in [12]. However, the multi-level conductance involved introduces programming noise and requires reprogramming for drift mitigation. Binary parameter storage with Monte-Carlo dropout-based inference [14] was used in [15], which while easier to train, are less expressive for out-of-distribution (OOD) data [16], [17].

Sparsity: Many of the aforementioned works implement dense BNNs, where all parameters are used to create ensembles. To improve ensembling efficiency, theoretical studies have explored partial Bayesian inference, which involves sampling only select parameters or layers for ensembles [18]–[20]. In binary networks, increased sampling sparsity (fewer probabilistic synapses) has been reported as training progresses [21] due to greater predictor confidence and reduced uncertainty for in-distribution (IND) data [22]. In hardware, [12] performs ensembling only in the fully connected (FC) layers after feature extraction by the convolutional layers. In [7] only the deepest layers were sampled, which improved hardware efficiency but resulted in a larger number of ensembles for the deepest layers, and a drop in accuracy was observed.

Contributions: The main contributions of this work as:

- We propose a sparsity-aware PCM-based in-memory computing (IMC) architecture optimization for Bayesian Binary Neural Networks (BBNNs) that leverages both layer sparsity (LS)—sampling only deep layers—and row sparsity (LS+RS)—sampling only rows with probabilistic synapses (Fig. 1). Simulation results show no loss in accuracy or uncertainty quantification compared to the FP32 baseline, and a simple drift compensation technique maintains performance stability up to 10^7 s.
- We use the NeuroSIM [23] simulator to project hardware efficiency, and achieve up to $5.3\times$ smaller area, $8.8\times$ power efficiency and $12.5\times$ total efficiency with LS only and $45\times$ with LS+RS, compared to non sparsity-aware implementation. We also achieve $2.9\times$ higher power efficiency compared to the state-of-the-art.

II. BACKGROUND

Bayesian Neural Networks: Given a BBNN parametrized by $\mathbf{w} \in \{-1, +1\}^{|\mathbf{w}|}$, Bayesian learning involves estimating the posterior $p(\mathbf{w}|\mathcal{D})$ which quantifies the likelihood of \mathbf{w} under the evidence presented by the training dataset $\mathcal{D} = \{x_i, y_i\}_i$. The trained weights then follow a posterior distribution $p(\mathbf{w}|\mathcal{D})$ rather than a single point-estimate [16].

Bayesian learning in BBNNs is performed through mean-field variational inference (VI) described in [21] to obtain a collection of synaptic probabilities $\mathbf{p}_w = \{p_w\}_{w \in \mathbf{w}}$ such that $p_w = Pr(w = +1)$. An ensemble of networks can be then created by sampling \mathbf{w} (Fig. 1) which can be accumulated during inference to obtain the final marginal predictor

$$p(y|\mathbf{x}, \mathcal{D}) = \frac{1}{N_{MC}} \sum_{i=1}^{N_{MC}} p(y|\mathbf{x}, \mathbf{w}_i). \quad (1)$$

Here N_{MC} refers to the number of sampled predictors combined in Monte Carlo fashion.

Aleatoric and Epistemic Uncertainty: The total uncertainty of the prediction U_{tot} for a given input x is calculated as prediction entropy as specified in [12]. U_{tot} is then decomposed into aleatoric uncertainty U_a quantifying the uncertainty emerging from the measurement noise of in-distribution (IND) data, and epistemic uncertainty U_e quantifying the inherent uncertainty in the model caused by limited evidence due to inadequate amount of data \mathcal{D} .

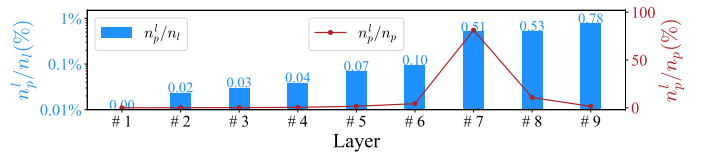


Fig. 2: Probabilistic synaptic parameter concentration across layers. The bar plot depicts the fraction of the layer that is probabilistic (n_p^l/n^l). The line plot shows the layerwise proportion of all probabilistic synapses (n_p^l/n_p).

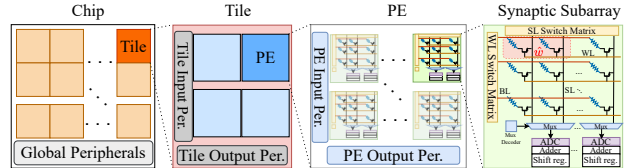


Fig. 3: The accelerator chip architecture, based on [23].

When all individual predictors $p(y|\mathbf{x}, \mathbf{w})$ agree, $U_e = 0$. Upon disagreement, it is positive indicating an out-of-distribution (OOD) input. Note that for traditional non-Bayesian frequentist networks with point estimate weights $U_{tot} = U_a$, and therefore $U_e = 0$.

PCM Devices: A phase change memory (PCM) device consists of a chalcogenide material such as $\text{Ge}_2\text{Sb}_2\text{Te}_5$ sandwiched between two metal electrodes. The device conductance is programmed using a write-and-verify scheme varying the programming pulse magnitude iteratively [24], [25]. PCM devices exhibit Gaussian-distributed programming and read noise with the former having a dominant effect, as well as a state-dependent drift in programmed conductance levels.

III. SPARSITY-AWARE PCM IMC ARCHITECTURE

In this section, we introduce the proposed sparsity-aware IMC optimization for PCM-based hardware architecture. We discuss the sampling sparsity in network and introduce LS and LS+RS schemes for BBNN accelerator architecture.

Sparsity: For a binary-valued synapse $w \in \mathbf{w}$ with $p_w = Pr(w = 1)$, $p_w = 0$ indicates that the synapse is always -1 , while $p_w = 1$ implies that it is $+1$. The extreme cases are deterministic synapses with fixed values across all samples, whereas the other synapses, that are probabilistic, take either value depending on p_w . Let n_d the total number of deterministic synapses and n_p total number of probabilistic synapses be n_p , with n_p^l denoting the number of probabilistic synapses in layer l and n^l the total number of synapses in that layer. Fig. 2 shows the fraction of stochastic weights in each layer (n_p^l/n^l), and the share of total probabilistic synapses per layer (n_p^l/n_p) for VGGBinaryConnect trained on CIFAR-100. We observe significant sampling sparsity in the network, i.e., $n_d \gg n_p$ [21]. To further increase sparsity, p_w near the extreme values were clamped to 0 or 1.

Chip Hierarchy: Fig. 3 shows the hierarchical structure of the NeuroSIM accelerator architecture [23]. The chip contains compute tiles, along with global buffers, accumulation, batch normalization (BN), and pooling units. Each tile maps weights

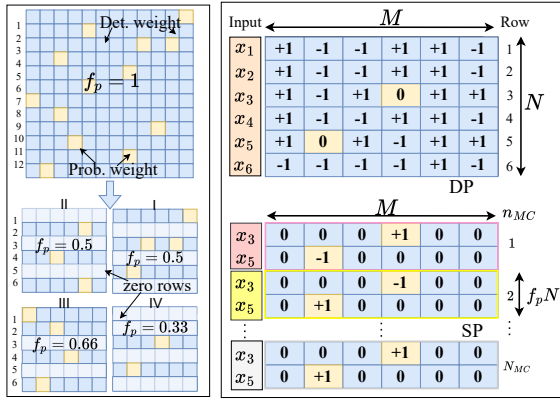


Fig. 4: **Left:** Partitioning matrix into W^D and W^S . Yellow-colored cells represent probabilistic synapses, while blue ones represent deterministic. **Right:** DP-SP split and MVM operation for submatrix IV. For an $f_p = 0.33$, the $N_{MC} = 10$ submatrices will require 4 subarrays. Inputs corresponding to non-zero rows are sliced and fed to each $W_{i,sub}^S$ of the SP.

from only a single layer, but multiple tiles can be used if the layer exceeds the tile size. Tiles are divided into processing elements (PEs), which house 1T-1R PCM crossbar synaptic subarrays.

Layer Sparsity (LS)-only scheme: Each probabilistic layer generates N_{MC} outputs according to (1), requiring multiple instantiations in subsequent layers regardless of sparsity. To minimize complexity, we select an appropriate first ensembling layer (FEL) with significant probabilistic synapses, ideally deep in the network. Based on Fig. 2, layer 7 is chosen as the FEL for this network. Synapses in earlier layers are clamped to 0 or 1, while only layers 7-9 are ensembled in space, with all N_{MC} samples processed in parallel.

DP-SP Architecture: To further increase area efficiency we exploit the inherent probabilistic sparsity in these layers by dividing and mapping them into a deterministic plane (DP) and the stochastic plane (SP). All the rows containing probabilistic synapses are extracted into sub-matrices and sampled to create ensembles. To generate the layer output for ensemble i , the DP outputs are combined with the output i^{th} submatrix in SP, as illustrated in Fig. 1.

To illustrate the splitting mechanism shown in Fig. 4, consider mapping a layer of the i^{th} network sample with weight matrix W_i , with the corresponding DP and SP counterparts represented as W_i^D and W_i^S . Each element $\hat{w} \in W_i^D$ is

$$\hat{w} = \begin{cases} w & \text{if } p_w \in \{0, 1\}, \\ 0 & \text{otherwise.} \end{cases} \quad (2)$$

Thus $W_i^D = W_j^D = W^D$ for all $i \neq j$. The probabilistic synapses are contained in W_i^S such that $W_i = W^D + W_i^S$ and an MVM operation for an input x is given by

$$y_i = W_i x = W^D x + W_i^S x. \quad (3)$$

As W_i^S is a sparse matrix, rows with no non-zero values can be removed before mapping. However, we observe that only a few rows of W_i^S are zero rows, as illustrated in Fig. 4, even though the rows themselves are sparse vectors. Empirically,

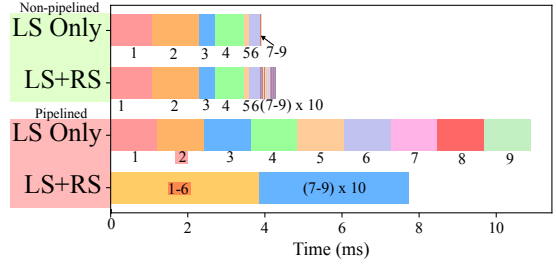


Fig. 5: Timing analysis for pipelined and non-pipelined mode for both LS and LS+RS modes. $\times 10$ highlights the 10 ensembles that are processed sequentially. Stage numbers highlighted in red in pipelined mode decide stage latency.

we observed that while the minimum sparsity in any row vector was around 98%, only 1.5% of all rows were zero rows. However, as each W_i^S needs to be split into submatrices corresponding to subarray dimensions before mapping, the smaller submatrices $W_{i,sub}^S$ have sufficient row sparsity (RS). The sparsity increases with decreasing subarray size. Hence, we can eliminate the zero rows and squeeze each submatrix before mapping to hardware. For example, if the fraction of non-zero rows in a submatrix, $f_p = 0.1$, then 10 ensembles can fit into one subarray. The fraction f_p is calculated for each subarray mapping to optimize packing.

To perform the MVM operation, an input subvector from x , corresponding to the non-zero row indices, is fed to the SP subarrays. Column sums accumulated in each local buffer (PE/tile) are then globally combined to obtain the final pre-neurons, which are passed to global BN, ReLU, and Pooling units. While column sparsity exists at the subarray level, squeezing columns causes misalignment, preventing parallel row readouts, and requiring extra circuitry and a more complex sparsity handling strategy [26].

For maximum area efficiency, both LS and RS schemes can be combined into LS+RS. With multiple ensembles packed into the same subarrays, PEs, and tiles, ensembling is done sequentially, unlike the parallelism in LS-only scheme.

Timing: Fig. 5 illustrates the timing strategy for both LS and LS+RS strategies in pipelining and non-pipelining modes. As discussed earlier, in the LS+RS scheme, predictions are available sequentially, trading latency for area efficiency compared to the LS-only scheme. However, we note that shallower convolutional layers require longer processing times than an FC layer due to the ‘slide-over’ operation of convolutional kernels and larger input feature maps [23] making additional latency per image minimal.

In pipelined LS-only mode, each layer functions as a pipeline stage, with stage latency set by the slowest layer, minimizing control overhead. In LS+RS mode, where layers 7-9 are processed serially, the same pipelining strategy would create stalls, as shallower layers would need to pause for ensemble processing in deeper layers. To address this, we propose a two-stage pipeline: layers 1-6 process in stage 1, and all ensembles for layers 7-9 complete sequentially in stage 2. For $N_{MC} = 10$, the shallow layers dominate the

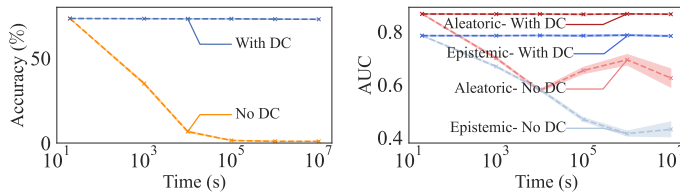


Fig. 6: Accuracy (Left) and AUC of ROC curves for aleatoric and epistemic uncertainty (Right) for CIFAR-100 dataset. The band around lines represent one standard deviation.

latency, so the two-stage LS+RS pipeline minimizes per-image latency, though the LS-only mode provides better throughput in pipelined operation due to reduced stage latency.

Weight mapping, operation, and drift compensation: Each weight of the network $w \in \{-1, 1\}$. In addition, many cells will be mapped to 0 as per (2). To avoid non-linearity due to drive voltage [27], row inputs are sequentially bit-streamed and the products are shift-added at every column for n cycles, where n is the input bit-width. Therefore, each synapse requires 2-bit storage resulting in two devices per cell, as shown in Fig. 3. The weight-to-conductance scaling is chosen to utilize the full dynamic range of conductances available for PCM devices (0-25 μ S).

As discussed earlier, the devices experience conductance drift with a state-dependent exponent ν . Since all devices store conductance values of either 0 or 25 μ S, the weights drift with the same nominal value of the exponent, reducing all pre-neuron values by approximately the same factor. To counter this, we periodically scale the BN coefficients to restore the pre-neurons to their nominal values. Unlike the common practice of subsuming BN coefficients into the synaptic layer by scaling the synapses [28], we apply BN layer separately to preserve the ternary nature of the weights.

IV. EXPERIMENTS AND CONCLUSIONS

We present the accuracy and uncertainty results on CIFAR-100 dataset with VGGBinaryConnect network transferred to a custom PCM simulator that incorporates device characteristics from [29] and the sparsity characteristics outlined here. We assess classification accuracy, uncertainty quantification, and stability under drift (Fig. 6). Additionally, we estimate area, energy, and latency using the NeuroSIM emulator [23].

Accuracy and Uncertainty Performance: To evaluate epistemic uncertainty, we use CIFAR-10 as the OOD data, given its mutually exclusive classes from CIFAR-100 [30]. Aleatoric and epistemic uncertainties are assessed using the AUC of the ROC curve. Aleatoric ROC specifies the ability to differentiate correct from incorrect IND data, while epistemic ROC characterizes IND vs. OOD discrimination capability [12].

We see minimal accuracy drop compared to the FP32 baseline (73.34% vs. 73.68%) despite clamping a few shallow-layer parameters. Drift compensation (DC) by scaling BN parameters completely recovers accuracy and aleatoric uncertainty performances for up to 10^7 seconds.

Hardware Projection: We estimate hardware performance by evaluating PCM IMC accelerator described here with

TABLE I: Hardware performance of various sparsity schemes

Parameter	No LS or RS	LS only	LS+RS
Pip.latency (per stage; ms)	1.43	1.43	4.00
Energy (mJ)/image	1.51	0.17	0.17
Area (cm²)	65.38	45.09	12.2
Throughput (FPS)	698	698	250
Power Eff. (FPS/W)	664	5722	5938
Total Eff. (Pip; FPS/W/cm²)	10.2	126.9	488
Non-Pip. latency (ms)	4.02	4.02	4.29
EDP (Jμs)	6.66	0.77	0.8
LEAP (Jms/μm²)	43.53	3.48	0.97

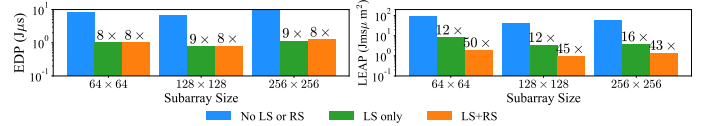


Fig. 7: EDP and LEAP for non-sparsity aware, LS only and LS+RS sparsity schemes. The labels on top of the bars indicate improvement over the non-sparsity-aware implementation.

128 \times 128 subarrays on 90 nm technology, a node chosen to match device characteristics in [29]. Throughput in pipelined mode is measured in frames per second (FPS), with power and total efficiency in FPS/W and FPS/W/cm² respectively. In non-pipelined mode, latency measures compute speed, with the energy-delay product (EDP) and latency-energy-area product (LEAP) used as figures of merit (FoMs). We achieve 2.9 \times higher power efficiency than the state-of-the-art reported in [7]. Table I shows hardware estimates. Both LS and LS+RS modes are around 8.8 \times more power-efficient than non-sparsity-aware implementations. LS+RS mode, with 3.7 \times smaller area, achieves 3.8 \times higher total efficiency than LS mode alone. In non-pipelined mode, LEAP improves by 12.5 \times in LS mode, with a further 3.6 \times gain in LS+RS.

Subarray size also impacts performance. Smaller subarrays reduce latency but at the cost of area and energy efficiency due to a smaller IMC-to-peripheral area ratio. Fig. 7 shows significant FoM improvements with sparsity. While EDP gains are minimal from LS to LS+RS, area reduction in RS results in a 3–4 \times increase in LEAP. We find 128 \times 128 to be optimal vis-à-vis both FoMs.

V. CONCLUSION

In this work, we presented two sparsity-aware BNN acceleration schemes: LS, which addresses layer-wise sampling sparsity, and RS, which exploits row sparsity. We achieved competitive accuracy on a PCM simulator, demonstrated uncertainty quantification, and effectively detected OOD samples. We also validated a simple drift compensation method completely recovering drift degradation of performance for up to 10^7 seconds. Our approach improves power efficiency by 8.8 \times and total efficiency by 12.5 \times (LS) and 45 \times (LS+RS). Similar gains were observed in non-pipeline mode.

We explored hardware efficiency trade-offs based on subarray size, finding 128 \times 128 to be optimal. While results may vary with different architectures and input sizes, the proposed schemes are adaptable to any convolutional or other BNN implementation.

REFERENCES

- [1] P. Shukla, A. Shylendra, T. Tulabandhula, and A. R. Trivedi, "MC²RAM: Markov Chain Monte Carlo Sampling in SRAM for Fast Bayesian Inference," in *2020 IEEE International Symposium on Circuits and Systems (ISCAS)*. IEEE, 2020, pp. 1–5.
- [2] C. Blundell, J. Cornebise, K. Kavukcuoglu, and D. Wierstra, "Weight uncertainty in neural network," in *International Conference on Machine Learning*. PMLR, 2015, pp. 1613–1622.
- [3] A. Kendall and Y. Gal, "What Uncertainties Do We Need in Bayesian Deep Learning for Computer Vision?" in *Proceedings of the 31st International Conference on Neural Information Processing Systems*, ser. NIPS'17. Red Hook, NY, USA: Curran Associates Inc., 2017, p. 5580–5590.
- [4] A. G. Wilson, "The case for Bayesian deep learning," *arXiv preprint arXiv:2001.10995*, 2020.
- [5] H. Jang, N. Skatchkovsky, and O. Simeone, "BiSNN: Training spiking neural networks with binary weights via Bayesian learning," in *2021 IEEE Data Science and Learning Workshop (DSLW)*. IEEE, 2021.
- [6] P. Katti, A. Nimbekar, C. Li, A. Acharyya, B. M. Al-Hashimi, and B. Rajendran, "Bayesian Inference Accelerator for Spiking Neural Networks," in *2024 IEEE International Symposium on Circuits and Systems (ISCAS)*, 2024.
- [7] A. Lu, Y. Luo, and S. Yu, "An algorithm-hardware co-design for Bayesian neural network utilizing SOT-MRAM's inherent stochasticity," *IEEE Journal on Exploratory Solid-State Computational Devices and Circuits*, vol. 8, no. 1, pp. 27–34, 2022.
- [8] H. Fan, M. Ferienc, M. Rodrigues, H. Zhou, X. Niu, and W. Luk, "High-Performance FPGA-Based Accelerator for Bayesian Neural Networks." IEEE Press, 2021, p. 1063–1068. [Online]. Available: <https://doi.org/10.1109/DAC18074.2021.9586137>
- [9] R. Cai, A. Ren, N. Liu, C. Ding, L. Wang, X. Qian, M. Pedram, and Y. Wang, "ViBNN: Hardware acceleration of Bayesian neural networks," *ACM SIGPLAN Notices*, vol. 53, no. 2, pp. 476–488, 2018.
- [10] W. A. Wulf and S. A. McKee, "Hitting the memory wall: Implications of the obvious," *ACM SIGARCH computer architecture news*, vol. 23, no. 1, pp. 20–24, 1995.
- [11] K. Yang, A. Malhotra, S. Lu, and A. Sengupta, "All-spin Bayesian neural networks," *IEEE Transactions on Electron Devices*, vol. 67, no. 3, pp. 1340–1347, 2020.
- [12] D. Bonnet, T. Hirtzlin, A. Majumdar, T. Dalgaty, E. Esmanhotto, V. Meli, N. Castellani, S. Martin, J.-F. Nodin, G. Bourgeois *et al.*, "Bringing uncertainty quantification to the extreme-edge with memristor-based Bayesian neural networks," *Nature Communications*, vol. 14, no. 1, p. 7530, 2023.
- [13] P. Katti, N. Skatchkovsky, O. Simeone, B. Rajendran, and B. M. Al-Hashimi, "Bayesian Inference on Binary Spiking Networks Leveraging Nanoscale Device Stochasticity," in *2023 IEEE International Symposium on Circuits and Systems (ISCAS)*, 2023, pp. 1–5.
- [14] Y. Gal and Z. Ghahramani, "Dropout as a Bayesian Approximation: Representing Model Uncertainty in Deep Learning," in *Proceedings of The 33rd International Conference on Machine Learning*, ser. Proceedings of Machine Learning Research, M. F. Balcan and K. Q. Weinberger, Eds., vol. 48. New York, New York, USA: PMLR, 20–22 Jun 2016, pp. 1050–1059.
- [15] S. T. Ahmed, K. Danouchi, C. Münch, G. Prenat, L. Anghel, and M. B. Tahoori, "Spindrop: Dropout-based Bayesian binary neural networks with spintronic implementation," *IEEE Journal on Emerging and Selected Topics in Circuits and Systems*, vol. 13, no. 1, pp. 150–164, 2023.
- [16] L. V. Jospin, H. Laga, F. Boussaid, W. Buntine, and M. Bennamoun, "Hands-On Bayesian Neural Networks—A Tutorial for Deep Learning Users," *IEEE Computational Intelligence Magazine*, vol. 17, no. 2, pp. 29–48, 2022.
- [17] A. Chan, A. Alaa, Z. Qian, and M. Van Der Schaar, "Unlabelled data improves Bayesian uncertainty calibration under covariate shift," in *Proceedings of the 37th International Conference on Machine Learning*, ser. Proceedings of Machine Learning Research, H. D. III and A. Singh, Eds., vol. 119. PMLR, 13–18 Jul 2020, pp. 1392–1402.
- [18] M. Sharma, S. Farquhar, E. Nalisnick, and T. Rainforth, "Do Bayesian neural networks need to be fully stochastic?" in *International Conference on Artificial Intelligence and Statistics*. PMLR, 2023, pp. 7694–7722.
- [19] A. Kristiadi, M. Hein, and P. Hennig, "Being Bayesian, even just a bit, fixes overconfidence in ReLU networks," in *International conference on machine learning*. PMLR, 2020, pp. 5436–5446.
- [20] S. Prabhudesai, J. Hauth, D. Guo, A. Rao, N. Banovic, and X. Huan, "Lowering the computational barrier: Partially Bayesian neural networks for transparency in medical imaging AI," *Frontiers in Computer Science*, vol. 5, p. 1071174, 2023.
- [21] X. Meng, R. Bachmann, and M. E. Khan, "Training binary neural networks using the Bayesian learning rule," in *International Conference on Machine Learning*. PMLR, 2020, pp. 6852–6861.
- [22] O. Simeone, *Machine Learning for Engineers*, 1st ed. Cambridge University Press, Nov. 2022. [Online]. Available: <https://www.cambridge.org/highereducation/product/9781009072205/book>
- [23] X. Peng, S. Huang, Y. Luo, X. Sun, and S. Yu, "DNN+ NeuroSim: An end-to-end benchmarking framework for compute-in-memory accelerators with versatile device technologies," in *2019 IEEE International Electron Devices Meeting (IEDM)*. IEEE, 2019, pp. 32.5.1–32.5.4.
- [24] S. R. Nandakumar, M. Le Gallo, I. Boybat, B. Rajendran, A. Sebastian, and E. Eleftheriou, "A phase-change memory model for neuromorphic computing," *Journal of Applied Physics*, vol. 124, no. 15, p. 152135, 2018. [Online]. Available: <https://doi.org/10.1063/1.5042408>
- [25] B. Rajendran, A. Sebastian, and E. Eleftheriou, "Building next-generation AI systems: Co-optimization of algorithms, architectures, and nanoscale memristive devices," in *2019 IEEE 11th International Memory Workshop (IMW)*. IEEE, 2019, pp. 1–4.
- [26] W. Yue, T. Zhang, Z. Jing, K. Wu, Y. Yang, Z. Yang, Y. Wu, W. Bu, K. Zheng, J. Kang *et al.*, "A scalable universal Ising machine based on interaction-centric storage and compute-in-memory," *Nature Electronics*, pp. 1–10, 2024.
- [27] P.-Y. Chen, D. Kadetotad, Z. Xu, A. Mohanty, B. Lin, J. Ye, S. Vrudhula, J.-s. Seo, Y. Cao, and S. Yu, "Technology-design co-optimization of resistive cross-point array for accelerating learning algorithms on chip," in *2015 Design, Automation & Test in Europe Conference & Exhibition (DATE)*. IEEE, 2015, pp. 854–859.
- [28] I. Pérez and M. Figueroa, "A heterogeneous hardware accelerator for image classification in embedded systems," *Sensors*, vol. 21, no. 8, p. 2637, 2021.
- [29] V. Joshi, M. Le Gallo, S. Haefeli, I. Boybat, S. R. Nandakumar, C. Piveteau, M. Dazzi, B. Rajendran, A. Sebastian, and E. Eleftheriou, "Accurate deep neural network inference using computational phase-change memory," *Nature Communications*, vol. 11, no. 1, pp. 1–13, 2020.
- [30] A. Krizhevsky, G. Hinton *et al.*, "Learning multiple layers of features from tiny images," 2009.